Attributing observed Greenland responses to natural and anthropogenic climate forcings

Heather J. Andres · W. R. Peltier

Abstract We attribute climate variability in four independent reconstructions of Greenland-average temperature and precipitation over the twentieth century. The reconstructions exhibit substantial differences in the timing and amplitudes of climate variations. Linear, empirical models of Greenland-average temperature and precipitation variations on multi-decadal timescales are established from a suite of Community Climate System Model 3 simulations of the preindustrial millennium. They are compared against observational reconstructions after being tested against simulations of the industrial and future periods. Empirical estimates of variations over the industrial and future periods are correlated at greater than 0.95 with simulated values. Greenhouse gas increases account for the majority of the temperature and precipitation increases after the mid-1900s. In contrast to the simulations, observed temperatures and precipitation do not increase until the mid-1990s. Thus, the empirical models over-predict the response to greenhouse gases over the twentieth century. We conclude that CCSM3 is not capturing processes that are proving important to Greenland surface conditions. Furthermore, modes of North Atlantic variability exhibit opposite relationships with some observations compared with the simulations. In those cases, reversing the sign of this component of variability yields significant correlations between the estimated and observed accumulation values.

H. J. Andres (✉) · W. R. Peltier
Department of Physics, University of Toronto, 60 St. George St., Toronto, ON M5S 1A7, Canada
e-mail: handres@atmosp.physics.utoronto.ca

1 Introduction

Increases in Greenland near-surface temperatures since the 1990s are thought to be driving increasingly rapid mass loss from the Greendland Ice Sheet (GrIS) through historically large summer melt extents and a lengthening of the melt season (Hanna et al. 2011, 2014; Box 2013). Time-dependent gravity measurements made by the GRACE satellites indicate that these surface mass losses are contributing significantly to global sea level rise (e.g. Peltier 2009; Luthcke et al. 2013; Velicogna and Wahr 2013). Such temperature increases are thought to be responses to anthropogenic climate changes due to greenhouse gas increases. However, in the absence of knowledge of natural variations in temperatures and precipitation over the GrIS, it is difficult to identify when anthropogenic climate forcings would have first contributed significantly to Greenland climate and what future conditions over the GrIS are likely to be. This paper examines the sensitivity of observed and simulated surface atmospheric conditions over the GrIS to natural and anthropogenic sources of climate variability, so that variations over the industrial period and extending into the future can be better understood and predicted.

Most observational studies of the responses of Greenland to internal and external climate forcings consist either of analyses covering many sites in Greenland over a few decades (e.g. Box 2002; Hanna and Cappelen 2003; Hanna et al. 2008; Frauenfeld et al. 2011) or a few deep ice core locations that cover an extended period of time (e.g. Chylek et al. 2012; Kobashi et al. 2013a, b). Models may

be employed to fill this data gap, whether they be reanalysis products (Hanna et al. 2008, 2011; Wake et al. 2009), regional climate models of varying resolution (Wake et al. 2009; Box et al. 2009, 2013; Fettweis et al. 2013) or global climate models (Andres and Peltier 2013, hereafter referred to as AP13). However, over the earliest periods, different methods yield substantially different reconstructions, particularly for precipitation (Hanna et al. 2011; Box 2013), and reconstructions remain much more accurate for Greenland averages than for different regions of the GrIS.

Volcanic eruptions decrease Greenland temperatures, particularly in the west, decrease precipitation, decrease runoff and increase GrIS surface mass balance for a few years following such events (Box 2002; Box et al. 2009; Hanna et al. 2005; AP13). The episodic nature of volcanic events is found to generate interdecadal temperature variability in Greenland (Box 2013), and is associated with 23 % of the ensemble-mean variability in North Atlantic sea surface temperatures (SSTs) on multi-decadal timescales based on earth system model simulations (Booth et al. 2012).

Solar insolation variations are negatively correlated with the difference between GISP2 ice core-derived temperatures and Northern Hemisphere temperature reconstructions over the past 4000 years (Kobashi et al. 2013a). Also, station temperature records across all of Greenland exhibit power at periods of approximately 11 years (Box 2002). Greenland-average temperatures and precipitation are significantly positively associated with Greenland-average insolation variations in a suite of preindustrial simulations (AP13), and total solar irradiance increases drive low-frequency increases in the North Atlantic Oscillation (NAO) after a lag of 40 years and low-frequency decreases in the Atlantic Meridional Overturning Circulation (AMOC) after 10 years in a different millennium simulation (Swingedouw et al. 2011).

The NAO is generally found to be negatively correlated with Greenland temperatures, and predominantly in the west (Box 2002; Fettweis 2007; Hanna et al. 2008; Fettweis et al. 2013; Kobashi et al. 2013b). However, these connections exhibit seasonal dependence (Fettweis 2007; Hanna et al. 2008, 2011; Frauenfeld et al. 2011), and their strengths vary with time (Hanna et al. 2008, 2011). In addition, temperature time series from western sites exhibit similar spectral properties on subdecadal timescales as the NAO (Box 2002). Fettweis (2007) detects significantly negative correlations between the NAO and precipitation on the western and south-eastern coasts of Greenland, and positive correlations in the north-east. Due to these regional differences, few correlations have been established with Greenland-average precipitation (Fettweis 2007; Hanna et al. 2011). Nevertheless, significant correlations have been detected between total Greenland accumulation and the winter NAO, although the signs and strength of these

correlations change (Box et al. 2013). AP13 find that stronger relationships can be established with the difference between the NAO and the East Atlantic pattern (EA) than with the NAO. They extract significantly negative relationships between the NAO–EA and Greenland temperatures and precipitation in all simulations, with stronger connections for Greenland temperatures than for precipitation, and stronger connections in lower-resolution simulations.

Sea ice cover, the Atlantic Multi-decadal Oscillation (AMO) and the AMOC are all strongly inter-related in simulations of the preindustrial millennium (AP13). Furthermore, they are significantly correlated (negatively, positively and positively, respectively) with Greenland-average temperatures and precipitation after lags of 1–11 years (AP13). Extensive sea ice cover is also thought to suppress local Greenland temperature variability, especially along the eastern coast of Greenland (Box 2002). The AMOC has been linked to periodicities on 20-yr timescales in southern and central Greenland ice cores, and intermittency in the spectra from the DYE-3 core over 4000 years has similar features to that of the simulated AMO (Chylek et al. 2012). In addition, North Atlantic SSTs are found to be strongly negatively correlated with Greenland accumulation from 1880 to 1939, and very weakly negatively correlated thereafter (Box et al. 2013).

No significant relationships have been detected between Greenland temperatures or precipitation and the El Nino-Southern Oscillation, the Pacific Decadal Oscillation (PDO) or the NAO+EA (Hanna et al. (2011); AP13).

No significant variations in either Greenland temperatures or precipitation have been attributed to anthropogenically-sourced greenhouse gas emissions and aerosols. However, AP13 demonstrate that the residual differences between a linear model estimate employing natural internal and external climate forcings and both Greenland-average temperatures and precipitation exhibit statistically significant increases midway through the twentieth century. These increases appear correlated with greenhouse gas increases, although the separate roles of greenhouse gases and anthropogenic aerosols remain unclear (AP13). Booth et al. (2012) demonstrate that anthropogenic aerosols are associated with 66 % of multi-decadal variability in North Atlantic SSTs in an ensemble mean of earth system model simulations over years 1860 to 2005. The indirect aerosol effects on clouds are necessary for capturing this SST response to aerosols (Booth et al. 2012).

Whereas in AP13 we describe the extent to which an ensemble of millennium timescale climate simulations can be employed to separate the forced contribution of Greenland variation from the internally-generated variability, here we focus upon the application of these analyses to a set of observational reconstructions. We generate empirical models relating Greenland temperatures or precipitation to the

natural climate forcings mentioned above as well as to natural variations in greenhouse gas radiative forcing. We test the effectiveness of the empirical models against simulations over the industrial period and two representative concentration pathways of future climate evolution. Then, we compare empirical estimates to observational reconstructions of Greenland-average temperatures and precipitation.

2 Materials and methods

2.1 Data

2.1.1 Observations

We employ four different reconstructions of Greenland temperatures and accumulation to identify robust features under the limitations of sparse, intermittent and regionally-limited data.

- *AND* Andersen et al. (2006) provide common Greenland δ^{18}O and accumulation time series extracted from three ice core records (DYE-3, GRIP and N-GRIP) covering years 191 to 1974. Temperature is extracted via averaging of δ^{18}O, and accumulation is extracted through another statistical method (Andersen et al. 2006). These datasets have 5-year precision, and δ^{18}O anomalies have been converted to temperature anomalies as in Johnsen et al. (1989).
- *BOX* Box et al. (2013) and Box (2013) Greenland-average temperature and accumulation time series over years 1849 to 2012 are reconstructed using in situ measurements, ice cores and regional simulations. The temperature datasets are updated from those presented in Box (2013) as described in the dataset documentation. Both temperatures and accumulation are now reconstructed using RACMO2 regional simulations and the methodology described in Box et al. (2013).
- *GHCN* NCDC/NESDIS/NOAA/U.S. Dept. of Commerce, Carbon Dioxide Information Analysis Center/Environmental Sciences Division/Oak Ridge National Laboratory/U.S. Dept. of Energy, and Office of Climatology/Arizona State University (1995, updated quarterly) and NCDC/NESDIS/NOAA/U.S. Dept. of Commerce (2012, updated monthly) provide monthly temperature data from fifteen stations and monthly precipitation data from sixteen stations around the coasts of Greenland. The data span years 1867–2011, although no single dataset covers all of these years and most include gaps. Where these gaps do not exceed one month, we interpolate anomalies in the months prior to and following the gaps to estimate their values. Data from northern Greenland stations begin no earlier than the 1930s.

- *20CR* Compo et al. (2011) Twentieth Century Reanalysis data provide 2° globally-gridded data on monthly time steps from 1871 to 2011. The reanalyses are generated by assimilating observed surface pressure records into an ensemble of 56 global numerical weather forecast model simulations that are each forced by observed sea surface temperatures and sea ice distributions (Compo et al. 2011). The final time series is the ensemble average (Compo et al. 2011), and thus reproduces only part of the variability in regions and periods with few observations available to assimilate. The average spread between ensemble members over Greenland decreases dramatically with time as the number of assimilated data points increases (see Figure OR.1 in Online Resource 1). Furthermore, the ensemble member spread varies significantly with location. In year 1872, the spread values vary between 0.001 and 12 °C for temperatures in grid cells over Greenland. Precipitation spreads vary 9–287 kg/m^2/mon. Such issues have produced storminess trends in the North Atlantic that are inconsistent with observations (Krueger et al. 2013). Consequently, we only include in our analyses grid cells with ensemble spread values lower than the highest values from 1970 onward.

GHCN and 20CR Greenland-average temperature and precipitation time series are generated by scaling regionally-averaged reference climatologies by anomaly averages for each year. For 20CR, the reference period is chosen to include all years after 1969, based on inspection of Figure OR.1. For GHCN, the reference period includes all years with at least twelve stations contributing data (1953–1971 for temperature and 1952–1955 and 1959–1970 for precipitation). Data in every grid cell are centred and normalized with respect to their monthly climatologies and standard deviations over the reference period to remove seasonal and some regional dependencies from the data. Annual averages and sums are then calculated for temperature and precipitation, respectively. Finally, area-weighted averages are performed over whatever stations or cells contain data each year. GHCN station area weights are generated by introducing a polar coordinate system centred at the areal centre of mass of Greenland with grid cell limits midway between stations. The final anomaly time series are re-normalized and un-centred by spatial averages of the reference standard deviations and climatologies.

The only GHCN station in the northeast quadrant of Greenland with data prior to the reference period has no data within the reference period. Its reference climatology is estimated as its mean value over available years shifted by the average change of all other datasets with coverage during both periods. Similarly, its standard deviation is scaled by the ratio of standard deviations from other

stations over the two periods. The reference seasonal cycle in this cell is defined to be the average of reference seasonal cycles from all other datasets in the same region of Greenland.

The difference between the NAO index and the EA is used here as a proxy for poleward shifts of the North Atlantic jet (Woollings et al. 2010). This association is described in more detail in AP13. We employ two different sea level pressure datasets and one set of publicly-available NAO and EA time series. The NAO and EA spatial modes are calculated from sea level pressures following AP13.

- *CPC* Monthly teleconnection indices for the NAO and EA are obtained from NOAA's National Weather Service Climate Prediction Centre (NOAA/NWS/CPC 2013a, b). They are calculated by rotated principal component analysis applied to monthly 500 mb geopotential height fields spanning years 1950–2012 (NOAA/NWS/CPC 2013c). We average over DJF.
- *HadSLP2* The Hadley Centre's monthly historical mean sea level pressure dataset version 2.0 is a globally-gridded dataset of 5° Cresolution covering years 1850–2004 (Hadley Centre for Climate Prediction and Research, Met Office, Ministry of Defence, United Kingdom 2000, updated monthly; Allan and Ansell 2006).
- *20CR* The dataset is described above. We perform no corrections to the sea level pressure data, since data is less sparse over the North Atlantic region than over Greenland and the NAO and EA are such dominant modes.

Two different approaches are employed with both simulated and observed sea level pressure data to generate the NAO and EA time series. Firstly, NAO and EA spatial modes are calculated from sea level pressures in each dataset and then projected onto the data to generate time series. Secondly, a single set of mode patterns is calculated from all simulated preindustrial sea level pressure data sets of a given resolution simultaneously. Time series are then generated by projecting these modes onto sea level pressure data from any simulation at that resolution or by interpolating to observed grids and projecting. Simulated NAO mode spatial patterns and time series are correlated at greater than 0.94 for these two approaches. Correlations with the station-based NAO definition, given here by the difference between standardized simulated sea level pressures in grid cells over Stykkisholmur (identified as between 65–75°N and 20–25°W) and Ponta Delgado (between 35–40°N and 25–30°W), are at 0.88 for both resolutions. Simulated EA spatial patterns are more sensitive to the calculation method, with their lowest spatial correlations equalling 0.55. Nevertheless, such pattern differences do not appear to affect the time series significantly, as their correlations

exceed 0.86 in all cases. Consequently, we see no evidence that the positions of these North Atlantic modes have shifted in an important way in simulations of the industrial or future periods.

HadSLP2 mode patterns (not shown) exhibit few significant differences with respect to the model patterns. However, the positions of the NAO–EA centres of action from 20CR (not shown) are shifted with respect to the model patterns. Furthermore, these 20CR pattern differences are associated with time series differences that exceed 95 % of those from time segments of the same length extracted from the preindustrial simulations. Nevertheless, the 20CR NAO–EA time series remain significantly correlated with each other regardless of calculation method.

2.1.2 Simulations

All of the simulations have been performed using Community Climate System Model (CCSM) version 3 (Collins et al. 2006). This model reproduces twentieth century Arctic sea ice trends better than most models in the Climate Model Intercomparison Project (CMIP) 3 database (Stroeve et al. 2007), and it predicts similar Arctic seasonally ice-free years to those from the Community Earth System Model 1 when forced by similar future emissions trajectories (Vavrus et al. 2012; Meehl et al. 2013). CCSM3 southern ocean climate characteristics are significantly different than observed (Vettoretti and Peltier 2013), but our focus here is restricted to the Northern Hemisphere. In addition, CMIP5 models in general have shown only slight improvements over CMIP3 models in the representations of climate variability (Flato et al. 2013).

We have created four sets of six simulations, covering preindustrial (850–1849), industrial (1850–1999) and future periods (2000–2099). Within each set, three of the simulations are performed at atmospheric and land spectral resolutions of T42 and three at T85. Two of the simulations differ by volcanic reconstruction (either Gao et al. (2008) or Crowley et al. (2008)). Trace gases and aerosols are held fixed in the third T42 simulation. The final T85 simulation is forced identically to another simulation, but is initialized from a different date.

The preindustrial millennium and industrial simulations are discussed in detail in AP13. The future simulations are initialized from the industrial simulations and are extended through two different emissions trajectories following Representative Concentration Pathways (RCPs) 4.5 and 8.5 (Smith and Wigley 2006; Clarke et al. 2007; Riahi et al. 2007; Taylor et al. 2009; Wise et al. 2009). They employ time-varying forcings for total solar irradiance, orbital configuration, trace gas concentrations, aerosol mass distributions and ozone mass distributions. Details for these forcings are provided in Online Resource 1.
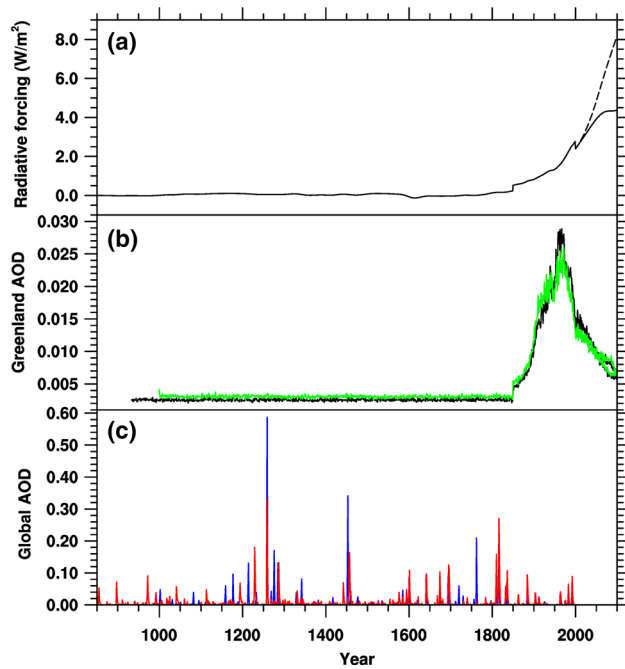
Fig. 1 External model forcings as a function of time. Greenhouse gas radiative forcing is plotted in **a**, anthropogenic aerosol optical depth averaged over Greenland in **b** and globally-averaged volcanic aerosol optical depth in **c**. In **a**, **b**, historical and RCP4.5 values are in *solid lines* and RCP8.5 are *dashed*. In **b**, T42 values are in *green* and T85 are in *black*. In **c**, Gao reconstructions are plotted in *blue* and Crowley in *red*

Fig. 2 External solar forcings as a function of time. Total solar irradiance in **a**, total orbital factor averaged over Greenland in **b** and solar insolation averaged over Greenland in **c**. T42 values are in *green* and T85 are in *black*

Total radiative forcings are shown with respect to year 850 values in Fig. 1a. These are calculated from the greenhouse gas concentrations supplied to the model for CO_2, CH_4, N_2O and CFCs 11 and 12 through radiative forcing equations provided in Ramaswamy et al. (2001). Increases in RCP4.5 greenhouse gas forcings diverge from RCP8.5 around year 2030 and flatten out by year 2060. Anthropogenic aerosol optical depths (AODs) averaged over Greenland are plotted in Fig. 1b. These forcings are held fixed over the preindustrial millennium, and show little resolution or RCP dependence afterward. Volcanic forcing time series are plotted in Fig. 1c and have been discussed in AP13. Note that we added data for the El Chichon event in 1982 to the Gao et al. (2008) volcanic reconstruction following the method in Gao et al. (2008) for a total loading of 14Tg H_2SO_4, which was provided in the dataset documentation. In reality, El Chichon aerosols remained mostly constrained to the Northern Hemisphere (Gao et al. 2008), so this modelling is expected to yield unrealistically large effects in the Southern Hemisphere.

Total solar irradiance and orbital forcings are plotted in Fig. 2 and are discussed in AP13. The rise in total solar irradiance over the twentieth century counteracts the steady

trend of -0.06 W/m^2 associated with orbital changes. Since no multi-decadal total solar irradiance variations are imposed over the future, solar insolation resumes following the orbital trend. Mean insolation values differ according to model resolution, but their anomalies are essentially identical.

2.2 Analyses

As in AP13, we develop empirical models of Greenland-average temperature and precipitation variations over the preindustrial period using lagged correlation and multiple linear regression analyses of simulated data. The preindustrial period is defined to span years 850 to 1799, so that smoothed anthropogenic AODs remain constant throughout the period. Further methodology changes are listed below.

The revised empirical model is defined by Eq. (1). The independent parameters include terms for globally-averaged volcanic AOD (volc), solar insolation (solar), the NAO–EA and greenhouse gas radiative forcings (GHG). X_ represent the smoothed time series for temperature (T), precipitation (Pr) and each of the independent variables. The linear coefficients are given by the $\beta_{T,\_}$ and the residuals by ϵ, and these are defined separately for Greenland temperatures and precipitation. The L_ terms represent the lags applied to these datasets in years.
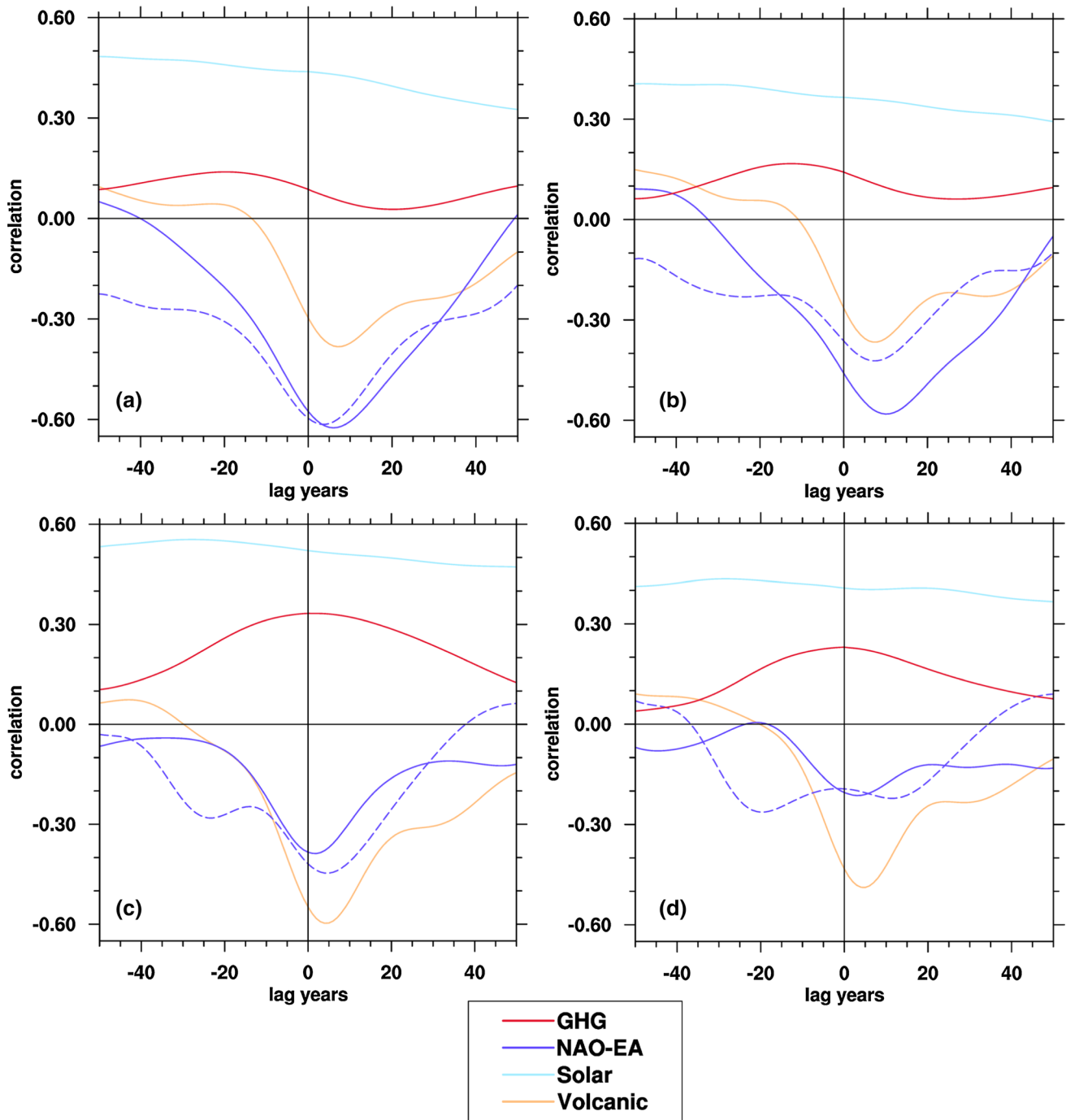
Fig. 3 Lagged correlations between Greenland temperatures (**a**, **c**) and precipitation (**b**, **d**) and all of the predictor variables included in the regression model after smoothing. Results for T42 shown in **a**, **b** and T85 in **c**, **d**. Predictor variable leading corresponds to a positive lag

$$
\begin{aligned}
X_T(t) = {} & \beta_{T,volc}X_{volc}(t - L_{volc}) + \beta_{T,solar}X_{solar}(t - L_{solar}) \\
& + \beta_{T,GHG}X_{GHG}(t) \\
& + \beta_{T,NAO-EA}X_{NAO-EA}(t - L_{NAO-EA}) + \epsilon_T(t)
\end{aligned}
\tag{1}
$$

Regression parameters are solved for using all datasets at a given resolution concurrently. Time series for a given variable at a given resolution are appended together into one long dataset with gaps placed between segments that exceed filter widths. All lagged correlations and regressions are performed on these long datasets. We estimate regression uncertainties at $p < 0.05$ in two ways. First, we scale the regression uncertainties to include effects from autocorrelations of the residuals (see AP13). Second, we apply

Table 1 Preindustrial regression coefficients and predictor lags employed in regression analyses based on correlation analyses

Response	Resolution	Volcanic		Solar		NAO–EA		GHG		R^2	Correlation	
		β	Lag	β	Lag	β	Lag	β	Lag	Preind	Preind	Anthro
Temperature	T42 full	**−0.32**	8	**0.30**	0	**−0.55**	3	0.06	0	**0.60**	**0.78**	**0.98**
	T42 natural											**0.74**
	T85	**−0.50**	4	**0.50**	0	**−0.25**	6	0.12	0	**0.70**	**0.84**	**0.98**
Precipitation	T42 full	**−0.30**	8	**0.26**	0	**−0.50**	7	0.09	0	**0.50**	**0.71**	**0.97**
	T42 natural											**0.68**
	T85	**−0.43**	5	**0.39**	0	−0.08	11	0.07	0	**0.40**	**0.63**	**0.95**

Statistically significant ($p < 0.05$) values are in bold font

bootstrapping techniques on 1000 separate sets of time series that span the preindustrial period. These sets of time series are constructed by randomly selecting data points from the original, unsmoothed time series while allowing for duplicate data point selection. Response datasets are sampled separately from the predictors, but the predictors are all sampled together in order to maintain any autocorrelations between them. These artificially-constructed datasets are smoothed and analysed in the same manner as the original time series.

Empirical model lags are determined through lagged correlation analyses over the preindustrial period using smoothed time series. We employ a Gaussian filter with a full-width-at-half-maximum value of 14 years, the choice of which is discussed in AP13. Lagged correlations are plotted in Fig. 3, where the predictor variable leading the response variable corresponds to a positive lag. Peak lag values are tabulated in Table 1 and are significantly different for the two model resolutions. We also perform lagged correlation analyses with the observational datasets for comparison (not shown). The observational data are prepared in the same way as the simulated data. We smooth all of the datasets with the same filter, except for AND, which has already been smoothed with a 5-year running mean filter. Similar spectral properties over multi-decadal timescales are recreated by smoothing AND with a Gaussian filter with a σ value of 5.8 instead of 6.0.

Two changes are made to the calculation of simulated Greenland-average temperatures and precipitation. First, Greenland boundaries are slightly altered from AP13 to include only the CCSM3 grid cells designated as land in the Greenland region. T42 grids include 115 cells with a total area of 2.39×10^6 km^2 and a mean altitude of 1200 m. T85 Greenland grids include 419 cells with a total area of 2.43×10^6 km^2 and a mean altitude of 1400 m. Thus, mean temperature differences presented in AP13 are unaffected. Second, we calculate Greenland-average precipitation rates instead of Greenland totals, since the average is much less sensitive to resolution differences in the Greenland area. Average precipitation rates at the two resolutions and their standard deviations agree until the twenty-first century.

Empirical estimates of Greenland-average temperature and precipitation changes over the anthropogenic period are generated by inserting time series for the independent variables from the industrial and future simulations and employing parameters established over the preindustrial period. Similarly, we generate estimates of observed Greenland-average temperature and accumulation changes by substituting observed NAO–EA variations into the regression model. In both cases, all of the time series are centred and normalized with respect to preindustrial means and standard deviations in order to be consistent with results obtained from the preindustrial period. As a result, coefficients of

Table 2 Normalization values over the preindustrial period for simulated and observational datasets and years of data available after smoothing

Dataset	Temperature (°C)				Accumulation (cm/a w. eq.)				
	Start year	End year	Mean	SD	Start year	End year	Mean	SD	SD/mean
T42	870	2079	−20.9	0.8	870	2079	38.2	1.4	0.04
T85	870	2079	−23.4	0.5	870	2079	38.9	1.1	0.03
AND	850	1954	0.0[a]	0.3	850	1954	1[b]	0.03[b]	0.03
20CR	1892	1991	−16.6	0.3	1963	1991	55	0.4	0.01
GHCN	1887	1991	−8.2	1.7	1894	1991	45.7	5.0	0.11
BOX	1860	1992	−19.9	0.6	1860	1992	41.3	1.6	0.04

For datasets with no data over the preindustrial, values are estimated using AND values over the preindustrial and anthropogenic periods. Further description is available in the text

[a] AND temperatures are anomalies, so they do not represent mean Greenland values

[b] AND accumulation is unitless, since it is calculated from locally-normalized accumulation rates

Fig. 4 Normalized Greenland-average **a** temperature and **b** precipitation anomalies plotted as a function of year for all observational datasets included in this study. Note that the year axis is magnified over the industrial period to make variations during that time clearer. All datasets have been smoothed, centred and normalized with respect to preindustrial values. Unsmoothed data is also included in *lighter colours*
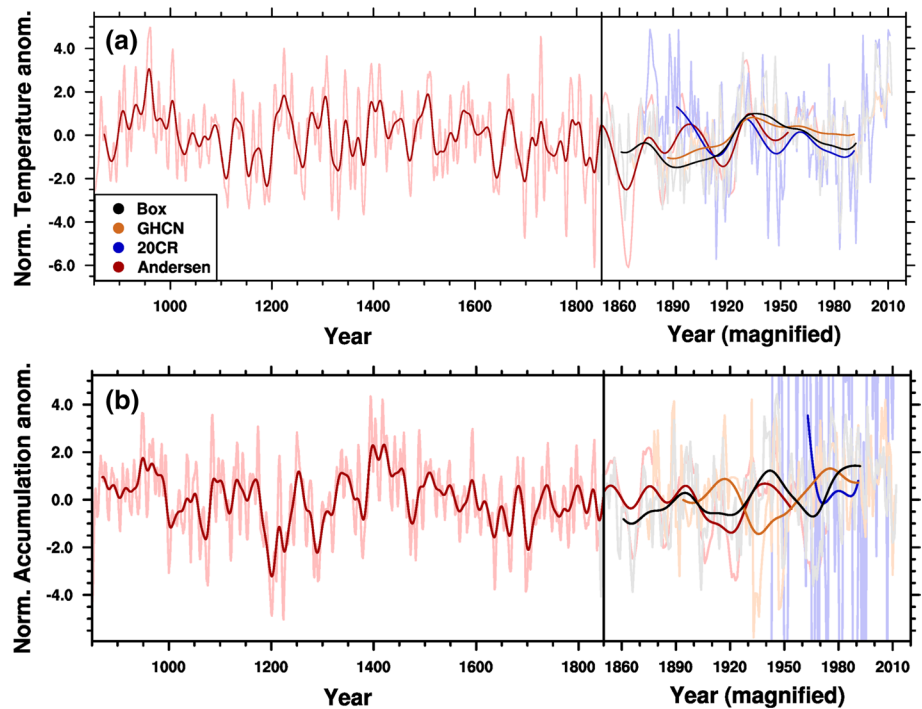
determination are not restricted to values of zero to one over the anthropogenic period, so we do not present them. Since AND is the only observational reconstruction with data in the preindustrial period, we estimate preindustrial means and standard deviations by matching changes in these properties for AND from the preindustrial to anthropogenic periods. Equations (2a) and (b) are applied over any overlapping years between AND and each of the other observational records. 20CR precipitation data does not overlap with AND after smoothing, so we use BOX with it.

$$\overline{T^{x}_{preind}} = \frac{\overline{T^{AND}_{preind}} - \overline{T^{AND}_{ind}}}{\sigma^{AND}_{ind}} * \sigma^{x}_{ind} + \overline{T^{x}_{ind}} \quad \text{and}$$

$$\sigma^{x}_{preind} = \frac{\sigma^{AND}_{preind}}{\sigma^{AND}_{ind}} \times \sigma^{x}_{ind} \quad (2a,b)$$

Since none of the NAO–EA observational time series have data in the preindustrial period, we estimate preindustrial normalization constants for them using Eqs. (2) with simulated NAO–EA time series in the place of AND. In this case, the overlap period ends in year 1999.

3 Results

3.1 Data characterization

Mean values and standard deviations for smoothed observational reconstructions estimated over the preindustrial

period are listed in Table 2. The ratio of accumulation standard deviations to their mean values tend to be constant (Andersen et al. 2006), so we also present those. All datasets but AND and BOX provide precipitation data instead of accumulation, which may affect the mean values and standard deviations. Due to AND temperatures being defined with respect to anomalies and AND accumulation being normalized with respect to local accumulation rates, only AND temperature standard deviations can be compared directly to the other datasets.

Observed temperatures and precipitation are warmer and wetter than the simulated values, although BOX values agree with simulated values. GHCN is subtantially warmer than the others, due to its reliance solely on coastal station data. The GHCN temperature standard deviation is also more than twice any other estimate. AND and 20CR provide the lowest temperature standard deviations. Accumulation mean values are all within 20 % of the reconstruction average. Differences are apparent in the accumulation standard deviations, especially with respect to mean values. AND, BOX and simulated ratios are all similar. GHCN and 20CR again stand out for large and small values, respectively.

GHCN temperatures and precipitation may exhibit high variability due to the small number of stations covering widely different regions of Greenland that are used to generate it. 20CR reconstructions contain relatively little power at low frequencies. Whereas smoothing reduces the standard deviations of all of the other datasets by a factor of 2 to 3, it reduces 20CR precipitation standard deviations
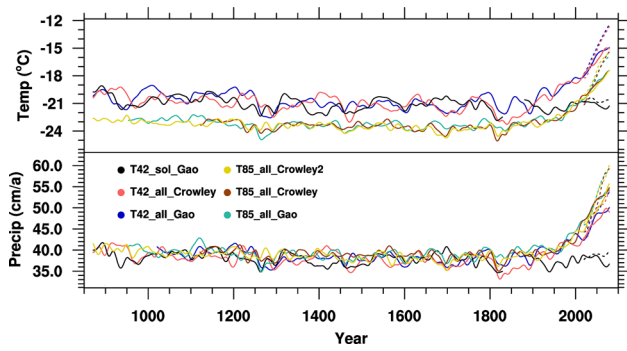
Fig. 5 Smoothed Greenland-average temperature and precipitation time series for all simulations. Historical and RCP4.5 time series are in *solid lines*, and RCP8.5 series are in *dashed lines*

by a factor of 14. Since both GHCN and 20CR reconstructions are defined in the same way, the method employed to generate these reconstructions does not appear to be robust to such features in the data.

Greenland-average reconstructions of temperature and accumulation variations are plotted in Fig. 4 after centering and normalizing. Anthropogenic temperature variations are small compared to AND preindustrial variations plotted in Fig. 4a. Nevertheless, all datasets with un-smoothed data covering the end of the twentieth century warm

dramatically beginning in the 1990s. This is consistent with a marked change in Greenland surface ice load beginning in this period inferred from a sharp change in the Earth's rotational state (Roy and Peltier 2011). Furthermore, all datasets exhibit warming during the 1920s followed by a gradual cooling leading into the 1990s. Overall, both AND and 20CR are significantly ($p = 0.05$) positively correlated with each other and the other temperature reconstructions prior to smoothing, and are insignificantly correlated with them afterward. GHCN and BOX are highly significantly correlated ($r > 0.9$, $p < 0.05$) both before and after smoothing.

AND accumulation oscillates regularly from the late eighteenth century until the early 1900s. During overlap years, BOX predicts similar signs of variations on similar timescales as AND with greater multi-decadal structure. They both indicate relatively dry conditions during the early 1900s followed by large increases in accumulation during the 1920s and 1930s. In contrast, the GHCN accumulation variations during this period are out of phase with AND and BOX. Greenland accumulation on the western coast occasionally varies out of phase with accumulation on the eastern coast (Box 2013), so the phasing differences may indicate that different regions are being emphasized in these datasets. Nevertheless, both GHCN and BOX exhibit increased accumulation at the end of the twentieth century

Fig. 6 Projections of NAO–EA modes onto sea level pressures at resolutions of **a** T42 and **b** T85. Smoothed NAO–EA time series for all simulations, where historical and RCP4.5 time series are in *solid lines* and RCP8.5 are in *dashed lines*
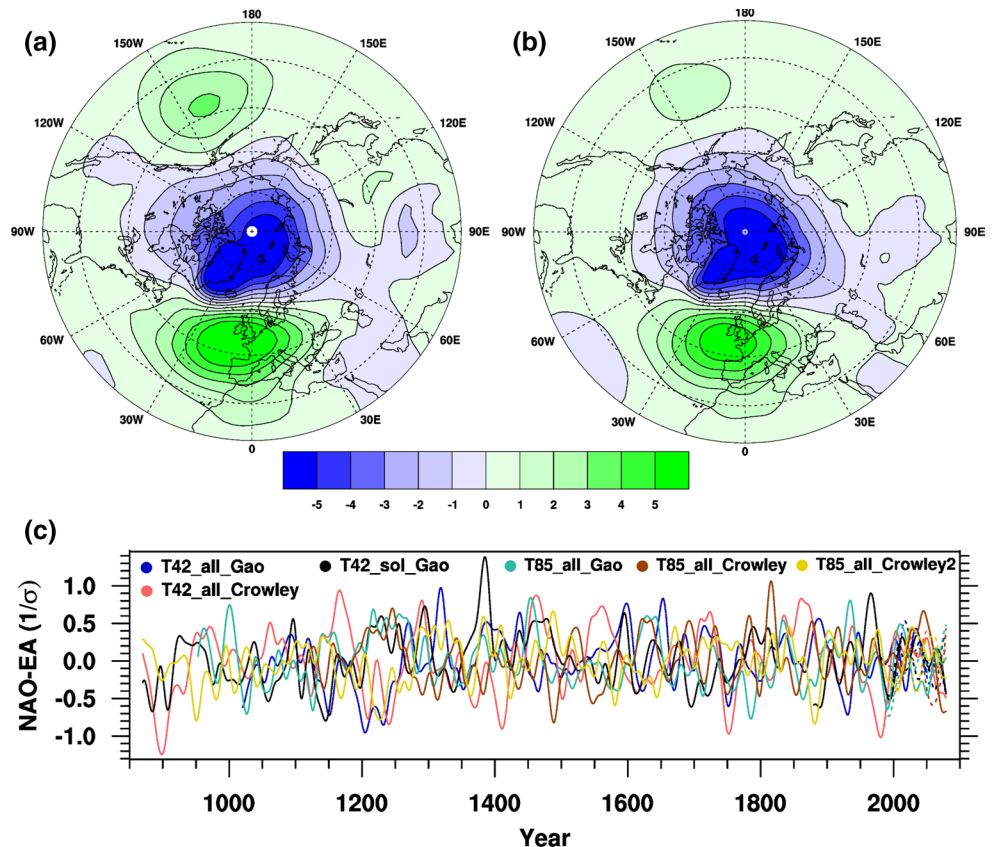
with respect to the start. The only structure in the 20CR precipitation record is a large decrease in precipitation in the 1960s followed by slightly increasing values, which is consistent with the Hanna et al. (2011) reconstructions also derived from 20CR precipitation data. Prior to smoothing, AND, 20CR and BOX are all significantly ($p < 0.05$) positively correlated over their respective periods of overlap. 20CR and BOX are also significantly positively correlated with GHCN. After smoothing, the only significant correlations are negative relationships between AND and GHCN.

Simulated Greenland-average temperature and precipitation time series are plotted in Fig. 5 after smoothing. Temperatures and precipitation from full-forcing runs exhibit significant increases at $p < 0.05$ from their preindustrial averages to averages over the last decade of the twenty-first century. These increases for temperature and precipitation are 5.8 °C and 9 cm/a for RCP4.5 and 7.7 °C and 11 cm/a for RCP8.5. In contrast, the natural forcing-only simulations (denoted T42_sol_Gao in Fig. 5) exhibit no significant temperature or precipitation differences over the same period. There are few significant changes in standard deviations between the preindustrial and anthropogenic periods, although standard deviations for Greenland temperatures in the natural-forcing only simulations are significantly lower ($p < 0.05$) over the twentieth century than over equivalent lengths of time sampled from the preindustrial millennium.

The NAO–EA spatial modes calculated from multiple preindustrial simulations at T42 and T85 resolutions are plotted in Fig. 6a, b. Smoothed time series for the NAO–EA based on projections of these modes onto simulated data are plotted in Fig. 6c. NAO–EA variability is significantly reduced ($p < 0.05$) during the future period for the natural-forcing simulations and insignificantly reduced for the fully-transient simulations. The biggest change in natural forcings during this period is the absence of volcanic eruptions, which suggests that there is a link between volcanic emissions and NAO–EA variability in this model.

Smoothed time series calculated directly for the HadSLP2, 20CR and CPC NAO, EA and NAO–EA modes are plotted in Fig. 7 in dark colours. Correlations between the NAO time series calculated from HadSLP2 and 20CR and based on the grid-cell definition described earlier all exceed 0.9, independent of approach. All reconstructions indicate that the NAO experienced sustained positive values from the 1900s to the 1930s followed by dramatic decreases to strongly negative values through the 1960s to the 1980s. The NAO then shifted as rapidly to predominantly positive values again. The different EA and NAO–EA time series are correlated above 0.85 prior to smoothing, and are only significantly correlated after smoothing when both time series are generated by projecting the same model modes. The EA exhibits little variability during the anthropogenic period except for a strong positive
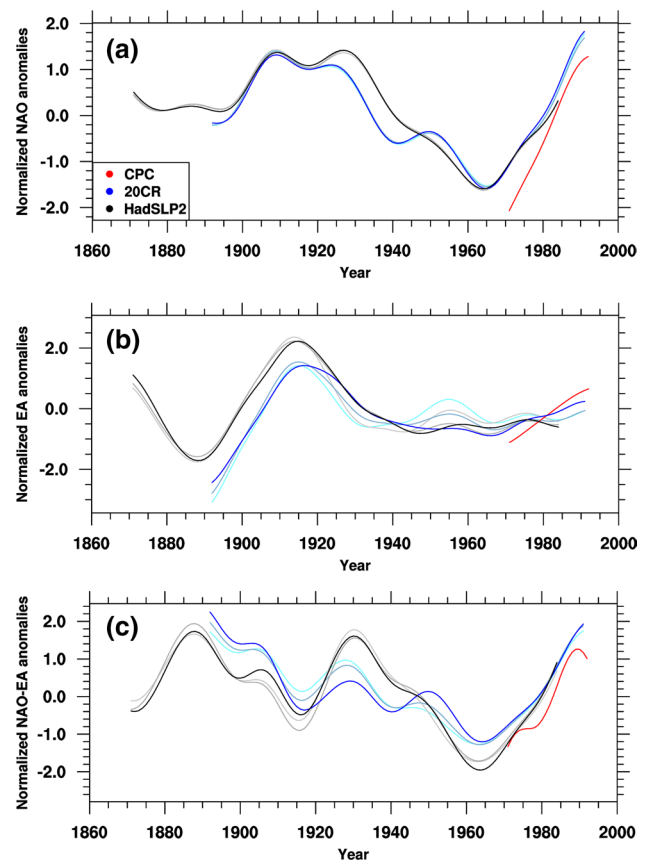
Fig. 7 **a** NAO, **b** EA and **c** NAO–EA anomaly time series for CPC, HadSLP2 and 20CR datasets. All have been smoothed and normalized with respect to preindustrial estimates from T85 modes. Modes calculated directly are in *dark shades*, with *lighter shades* corresponding to time series based on projected model modes

phase from 1910 to 1930 preceded by a similarly negative phase. The common NAO–EA patterns indicate that the NAO–EA shifted from generally positive values in the late nineteenth century to strong negative values during the 1960s and 1970s, followed by a shift again to positive values. The main differences pertain to its behaviour from 1920 to 1940. HadSLP2 predicts a phase of positive values during this time, whereas 20CR suggests weakly negative values. The sources of this discrepancy lie in the timing of the recovery from positive phases of the NAO and EA during the 1920s. The CPC time series is too short to extract more than a multi-decadal trend over its duration, but this trend is consistent with the other two datasets.

3.2 The empirical model

In preindustrial millennium simulations, we extract statistically significant ($p < 0.05$) correlations between smoothed Greenland temperatures and precipitation and smoothed

volcanic AOD, solar insolation, NAO–EA, and greenhouse gas radiative forcings. The lagged correlation relationships between these variables are plotted in Fig. 3, and the years of peak correlations are listed in Table 1 as lags with two exceptions. Except for solar insolation, all lags are longer than those in AP13.

First, solar insolation and the NAO–EA exhibit the only significant cross correlations between predictor variables over the preindustrial period at the lags examined. Thus, we plot lagged correlations between the NAO–EA and Greenland conditions extracted from control simulations with no external forcings applied in dashed purple lines in Fig. 3. The timing of peak correlations are shifted with respect to the transient runs, so we include lags from the control runs in Table 1. Second, greenhouse gas correlations are strongest in the T42 simulations when they lag behind Greenland conditions by 10–20 years. Nevertheless, during the anthropogenic period, correlations between greenhouse gases and T42 Greenland temperatures and precipitation exceed 0.97 ($p < 0.05$) when the datasets are in phase. Thus, we set the lag for the greenhouse gas term in calculations with T42 datasets to zero.

Preindustrial regression coefficients are presented in Table 1 along with corresponding R^2 values and correlations between the estimated time series and those extracted directly from the preindustrial simulations. In addition, correlation values are presented which have been obtained by applying the empirical models to simulations of the anthropogenic period. The empirical model parameters and preindustrial R^2 values presented in Table 1 for volcanic, solar and NAO–EA terms agree with most of those in AP13 within uncertainties.

Confidence intervals for the regression coefficients based on estimating effective degrees of freedom do not exceed ±0.08 for temperatures and precipitation at T42 resolution and ±0.06 and ±0.11 for temperatures and precipitation, respectively, at T85. Confidence limits determined through bootstrapping are all near to but less than ±0.17. The large differences in confidence interval estimates may be associated with difficulties in estimating the effective number of degrees of freedom in the residuals. These estimates are calculated by summing over auto-correlations in the residual time series until the auto-correlations turn negative (AP13). However, the timing of this cutoff can be very sensitive to small changes in autocorrelation values. For example, although T85 temperature and precipitation auto-correlations both exhibit initial minima by 35 years lag, the precipitation minimum is above zero. Hence, the cutoff for precipitation is at approximately 150 years. Due to this ambiguity, we highlight significant values in Table 1 in bold font using bootstrap estimates.

Preindustrial R^2 and correlation confidence limits at $p < 0.05$ are determined using bootstrapping methods as

well. They have upper values of 0.07 and 0.27, respectively. Correlations for the natural-forcing only simulations over the anthropogenic period are within uncertainties of those over the preindustrial period. Consequently, we conclude that the natural components of the regression models continue to predict Greenland temperatures and precipitation equally well over the anthropogenic period when greenhouse gases and aerosols are held fixed. In the fully-transient cases, the correlations are higher, indicating an improvement in predictive skill.

Correlation and regression analyses indicate that global volcanic AODs exhibit strong cooling and drying effects over Greenland after 4–8 years at both resolutions. Similarly, increased solar insolation leads to higher temperatures and precipitation over Greenland at both resolutions. Finally, positive NAO–EA states are associated with cooler, drier conditions over Greenland after lags of 3–7 years in the T42 simulations. Although positive NAO–EA states are associated with lower temperatures over Greenland at T85, it is much weaker than in the T42 simulations. The relationship with precipitation is not significant at a 95 % confidence level. These differences suggest that the mechanisms whereby internal variability drives conditions in the North Atlantic may be different at these two resolutions.

The regression relationships with greenhouse gases are not significant according to bootstrapping estimates. This result is inconsistent with the significant correlations extracted from T85 Greenland temperatures and precipitation over the preindustrial period. Nevertheless, the preindustrial greenhouse gas term is seen to well reproduce the substantial simulated temperature increases over the anthropogenic period in Fig. 8, where Greenland temperature and precipitation estimates are decomposed into their separate components for a selection of simulations. It also reproduces precipitation increases at T42 resolution and underestimates those in precipitation at T85. The contributions from greenhouse gases first exceed the 95 % range of total preindustrial variability by years 1974 and 1956 for T42 Greenland temperatures and precipitation, respectively. In T85 simulations, the 95 % threshold is exceeded by years 1945 and 1978. These estimates are much earlier than detected in observational analyses (e.g. Hanna et al. 2008; Roy and Peltier 2011).

Over the anthropogenic period, solar insolation contributes very little to multi-decadal variability in either simulated Greenland temperatures or precipitation. Volcanic eruptions only appear to have substantial effects over the early part of the anthropogenic period. The NAO–EA mode, however, plays an important role in Greenland temperature and precipitation estimates at T42 resolution.

Residuals from the anthropogenic period are plotted in Fig. 9. Dark grey shading indicates the range of 95 % of residuals from the preindustrial period, and light grey

Fig. 8 Plots of simulated Greenland temperature and precipitation anomaly time series with the components contributed by each regression model variable. Components are labelled in each plot, along with the total empirical estimate and response. Temperature is in plots **a** and **b** for T42_all_Crowley with RCP8.5, and T85_all_Crowley with RCP4.5. Precipitation is plotted in **c** and **d** for T42_sol_noO3_Gao with no RCP-specific forcings and T85_all_Gao with RCP8.5
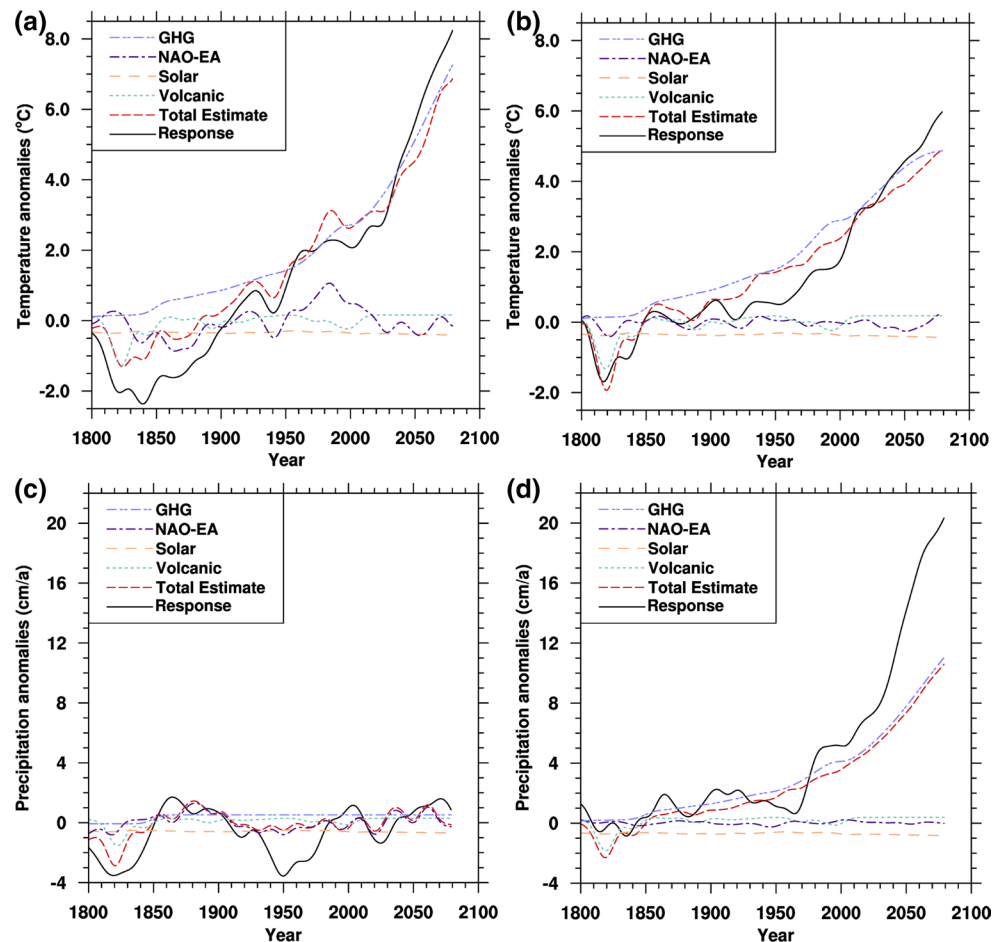
shading indicates 95 % confidence intervals for predicted values based on the regressions. The widening of the prediction bounds with year is due to an anticipated increase in estimated variance as a result of greenhouse gas radiative forcings being far from their preindustrial mean values (Sen and Srivastava 1990). All of the residuals remain within the 95 % prediction bounds, except for T42_all_Crowley precipitation residuals being occasionally low. However, both T42 temperature and precipitation residuals begin low with respect to preindustrial residuals, even in the natural forcing simulations. T42 temperatures increase to anomalously positive values by the end of the twenty-first century. T85 temperature and precipitation residuals begin within the range of preindustrial residuals and then decrease to the mid-twentieth century, followed by increases to anomalous values in the mid- and early twenty-first century, respectively.

In Fig. 9, the residual increases in temperature or precipitation are of the same magnitude for both RCPs 4.5 and 8.5. However, the temperatures and precipitation themselves increase roughly 2 °C and 2 cm/a more by year 2080 for RCP8.5 than for RCP4.5 at both resolutions. Thus, the linear model is accounting for most of the scenario-sensitive

components of the late twenty-first century warming. The residual components appear insensitive to representative concentration pathway and may reflect forcings not included in the empirical model, such as anthropogenic aerosols and ozone concentrations, or nonlinearities associated with circulation changes around Greenland. Ozone variations given by the differences between residuals from T42_sol_Gao simulations and an otherwise identical simulation with fixed ozone (plotted in light grey in Fig. 9a, c) do not reproduce the residual variations in the fully-transient runs. The direct effect of anthropogenic aerosols provides a candidate explanation, as anthropogenic AODs are significantly negatively correlated with T85 temperature residuals. However, anthropogenic AODs also exhibit significantly positive correlations with T42 temperature residuals and significantly negative correlations with precipitation residuals when they lag by more than 10 years.

3.3 Comparisons between observations and empirical estimates

Few correlations with AND over the preindustrial period are significant. AND preindustrial temperatures exhibit

Fig. 9 Differences between simulated Greenland temperature (**a**, **b**) and precipitation (**c**, **d**) and their empirical esimates for T42 (**a**, **c**) and T85 (**b**, **d**). Time series for RCP4.5 are in *solid lines*, and RCP8.5 are in *dashed lines*. *Dark grey shading* indicates 95 % confidence limits from residuals over the preindustrial period, and *light grey shading* corresponds to 95 % CIs for predicted values based on regressions
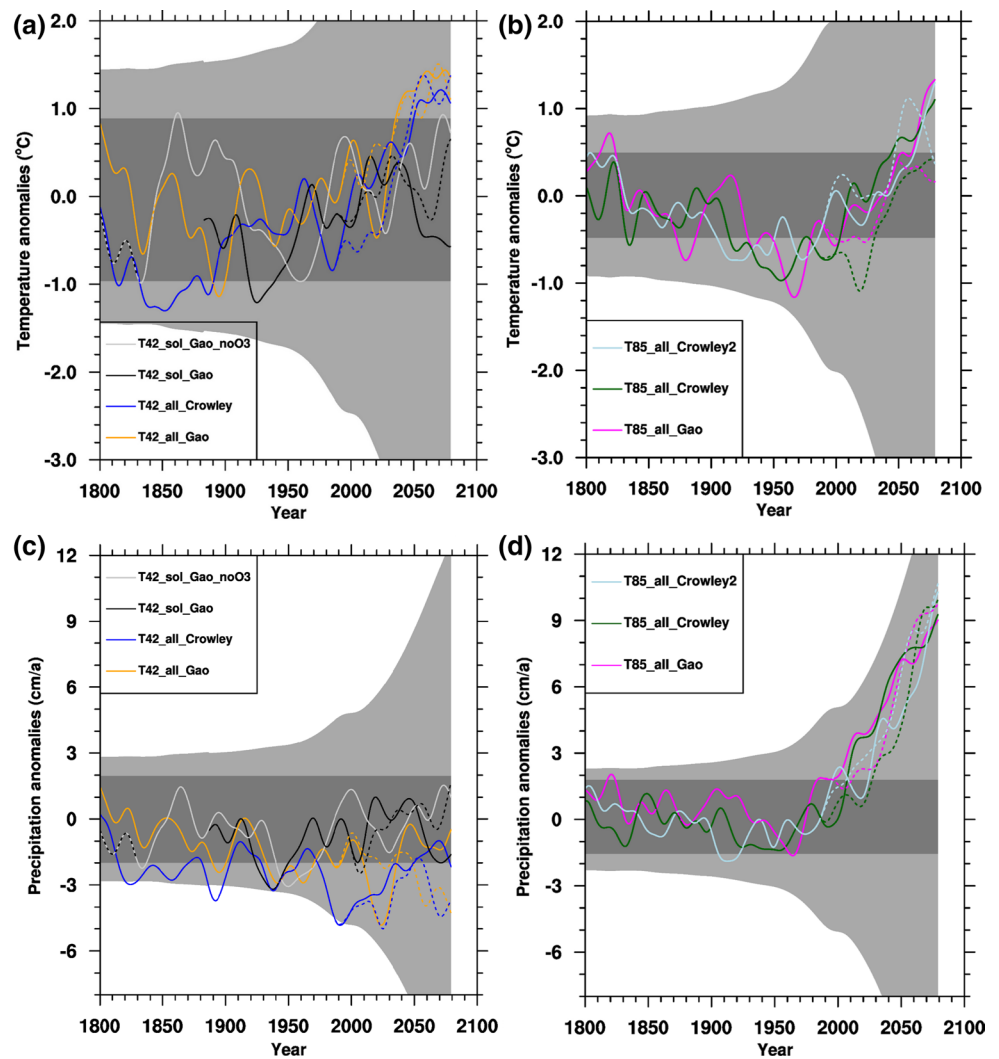
significant, positive correlations with AND accumulation after a lag of 7 years. Significant predictor correlations are detected between AND accumulation and volcanic AODs, such that both volcanic reconstructions are negatively correlated ($p < 0.05$) with AND accumulation after being lagged by 26–28 years. In addition, AND temperatures are significantly positively correlated with solar insolation after a lag of 29 years. All of these peak lag times are substantially longer than those obtained from the simulations. Otherwise, some correlations exhibit consistent patterns between reconstructions. AND temperatures are negatively correlated with volcanic AODs and display minima when volcanic time series lead temperatures by 3–10 years. Similarly, correlations with insolation are positive, and correlations with greenhouse gases are negative. None of the NAO–EA time series have data during the preindustrial period.

Over the anthropogenic period, many of the predictor variables are cross-correlated, which makes identiying their separate influences difficult. None of the

Greenland temperature or accumulation time series are significantly correlated with the volcanic reconstructions. However, we do detect significantly positive correlations between solar insolation and both GHCN and BOX temperatures when the solar insolation lags behind temperatures by 14–17 years. This result is attributable to cross correlations between solar insolation and the NAO–EA. Lagged correlations with the various NAO–EA time series exhibit occasional significance at $p < 0.05$ (particularly for GHCN and BOX time series), and they exhibit some consistent patterns of correlations. Correlations between the NAO–EA and Greenland temperatures are generally positive when the NAO–EA leads and generally negative when the temperature leads. The pattern is less consistent for accumulation. These common patterns indicate a marked departure from the results obtained with the simulations. Neither greenhouse gases nor anthropogenic AODs exhibit significant correlations with either Greenland temperatures or accumulation over the anthropogenic period.

Fig. 10 Residuals for observed temperatures in **a** and **b** and observed accumulation in (**c**) and (**d**). *Different colours* correspond to different Greenland temperature or accumulation reconstructions as labelled. *Solid lines* indicate residuals from regressions employing NAO–EA time series based on HadSLP2 data, and *dashed lines* indicate regressions employing NAO–EA time series based on 20CR data. All other variations in regression models (i.e. different volcanic reconstructions, different RCPs) are plotted in different lines. *Dark grey shading* indicates 95 % of simulated preindustrial residuals, and *light grey shading* indicates the 95 % confidence bounds based on prediction using the regression model
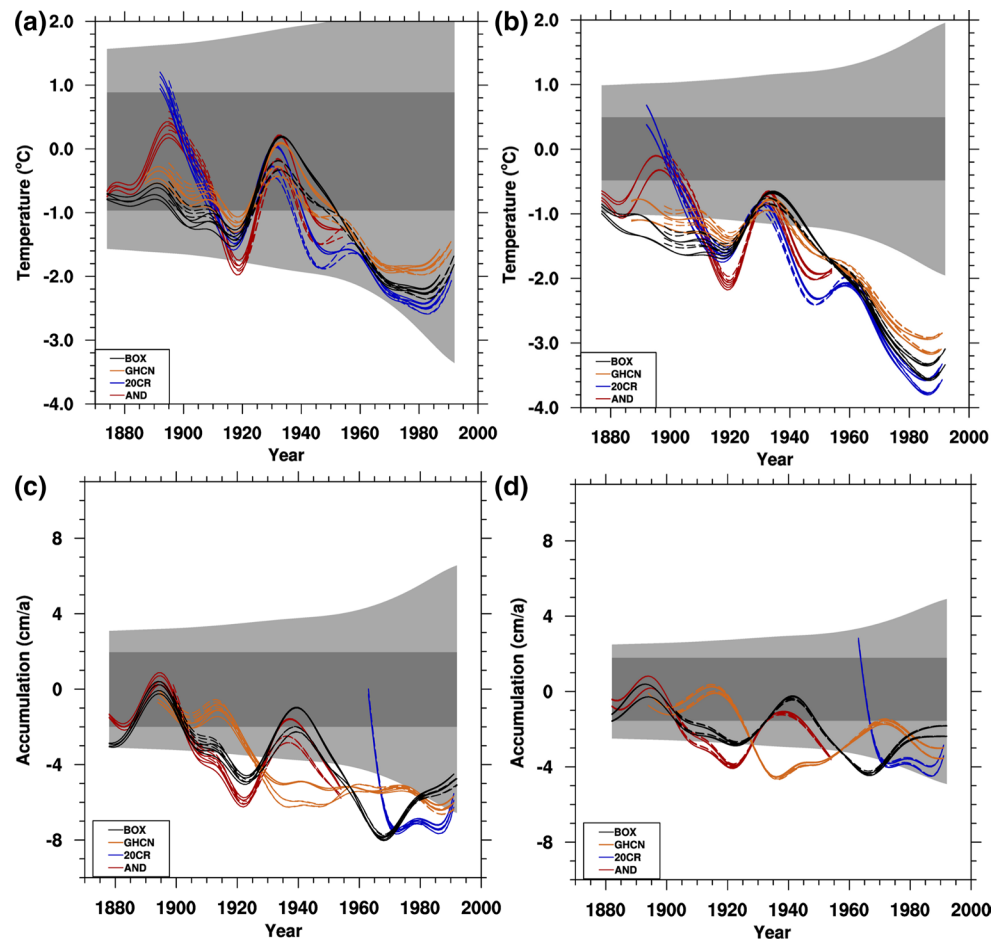
The empirical estimates of observed Greenland temperatures and accumulation based on Eq. (1) are not significantly correlated with the observational reconstructions of Greenland temperatures or precipitation. Nevertheless, when only solar and volcanic terms are included in the empirical estimates, correlations for Greenland temperatures are significant at both resolutions for AND, GHCN and BOX. Correlations with the highest significance are obtained with the Crowley volcanic reconstruction rather than the Gao reconstruction. No correlations are significant between accumulation reconstructions and the solar-volcanic model, which is consistent with lagged correlations for accumulation and these predictors being much different than from the simulations. Nevertheless, when the estimates are calculated using volcanic and solar terms with the lags based on AND lagged correlations over the preindustrial period, the accumulation estimates become significantly correlated with AND reconstructions, but not with any of the other time series. Thus the poor performance of the empirical estimates for accumulation are not restricted to solar and volcanic lags.

Including either the NAO–EA or greenhouse gas term does not improve the accuracy of the estimates. Instead,

correlations only remain significant in a few cases when the estimates are based on the volcanic, solar and NAO–EA terms. These cases include GHCN and BOX temperatures with the T85 parameters including the Crowley volcanic and HadSLP2 NAO–EA reconstructions. Note that the T85 regression model includes weaker terms for the NAO–EA than the T42 model. On the other hand, adding the greenhouse gas term makes correlations between the estimated and observed time series insignificant in all cases except BOX accumulation. Interestingly, the volcanic and solar components on their own do not produce an estimate that is significantly correlated with BOX accumulation, so the greenhouse gas term increases the significance of the comparison in this case.

Residual differences between the response variables and the full empirical estimates are plotted in Fig. 10. Each colour corresponds with a different response time series, and solid lines are associated with empirical estimates employing HadSLP2 NAO–EA time series, while dashed lines are associated with 20CR NAO–EA time series. As in Fig. 9, dark grey shading indicates the range of 95 % of simulated residuals over the preindustrial period, and light grey shading indicates the confidence bounds based on prediction

Fig. 11 Accumulation time series for **a** BOX and **b** GHCN plotted with regression estimates assuming the relationship between the NAO–EA and Greenland accumulation is positive. Estimates are provided for the Gao volcanic reconstruction and HadSLP2 NAO–EA modes based on projecting T42 simulated modes for RCP4.5
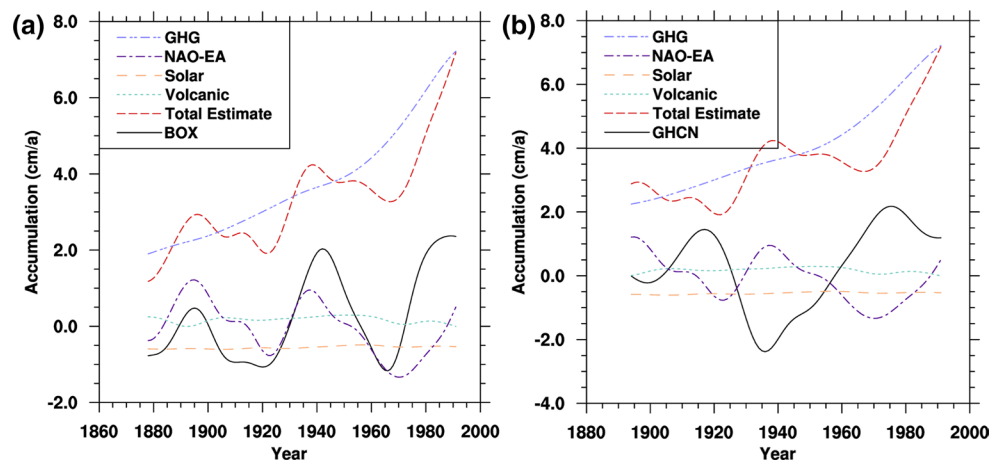
statistics using regression models (Sen and Srivastava 1990). The observed residuals are inconsistent with the regression model predictions except for temperatures using the T42 model. They are all lower than the range of simulated preindustrial residuals, particularly near the end of the twentieth century. These negative residuals are associated with over-predictions of the local response to greenhouse gases, as the residuals generally lie within the preindustrial range when only the volcanic, solar and NAO–EA terms are included in the estimate.

Switching the sign of the NAO–EA term in the empirical estimates employing the full models improves comparisons with reconstructed temperatures and accumulation for both AND time series and for BOX accumulation. In fact, correlations for BOX accumulation using the full empirical model become significantly positive in nearly all T42 cases. Decomposing the separate components for one of these cases in Fig. 11a demonstrates that the NAO–EA is highly positively correlated with BOX accumulation. The greenhouse gas term creates a positive offset between the estimate and the reconstructed values, but it also reproduces some of the accumulation increases beginning in the 1960s. Box et al. (2013) demonstrates that the sign of the relationship between the NAO and Greenland accumulation changes on numerous occasions throughout the twentieth century. We find no evidence of that here in the relationship with the NAO–EA. Instead, we note that in Fig. 7 during the main period that Box et al. (2013) detects negative correlations, namely years 1880 to 1940, the variations in the EA are negatively correlated with BOX accumulation. Thus, we conclude that the NAO–EA provides a more accurate representation of Greenland accumulation variability than the NAO alone.

Empirical estimates become significantly less correlated with GHCN temperatures and precipitation when the sign of the NAO–EA is changed. Correlations between GHCN accumulation and empirical estimates with all terms but greenhouse gases become significantly negative. One case is plotted in Fig. 11b, and shows that the NAO–EA is highly negatively correlated with GHCN precipitation. Thus, we see that the out-of-phase variations between GHCN and AND or BOX previously attributed to regional sensitivities in the reconstruction methodologies also correspond to variations in the NAO–EA.

4 Discussion

We demonstrate that the anthropogenic period (beginning in year 1800) is too short a time to establish many significant relationships between observational reconstructions of Greenland temperatures or precipitation and internal and external climate forcings on multi-decadal timescales. The anomalous and highly-correlated increases in emissions of greenhouse gases and anthropogenic aerosols over this period particularly confound such attempts. Empirical estimates of Greenland-average temperature and precipitation changes based on analyses of preindustrial millennium simulations show considerable skill at predicting simulated variations over the anthropogenic period. However, they do not show comparable skill at reproducing historical variations in Greenland temperatures or precipitation.

The four different reconstructions of historical Greenland temperatures and accumulation examined in this study are based on different observational records and employ different methodologies. These reconstructions exhibit significant differences in both their mean values as well as their patterns and amplitudes of variability. In particular, 20CR and GHCN include anomalously low and high temperature and precipitation variability, respectively. GHCN precipitation variations are also out of phase with respect to the other datasets during some periods. Phase differences may be evidence of sensitivities in the reconstruction methods employed to regional climate signals, and

these differences are significantly correlated with NAO–EA changes. Three different NAO–EA reconstructions are also employed for this period, and they are very similar except for their estimates of the amplitude and duration of increases from the 1920s to the 1940s.

Empirical estimates for Greenland-average temperatures and precipitation are defined through linear combinations of volcanic aerosol optical depth, solar insolation, the NAO–EA and greenhouse gas radiative forcing. The weights for each of these variables are established through multiple linear regression of data extracted from global simulations covering the preindustrial period. The empirical estimates lie within the 95 % predictive range of simulated Greenland temperatures and precipitation over the anthropogenic period (1800–2099 years). However, the residual differences exceed the 95 % range of residuals from the preindustrial period midway through the twenty-first century, or even earlier for higher-resolution precipitation. Greenhouse gases are associated with the largest component of climate variability during the anthropogenic period, and their contributions first significantly exceed background variability in the lower-resolution simulations by 1974 and 1956 years for Greenland temperatures and precipitation, respectively. The years are 1945 and 1978 for higher-resolution temperatures and precipitation, respectively. These results suggest that the influence of anthropogenic greenhouse gases are expected to have been important to Greenland surface conditions much earlier than previously thought.

In contrast to simulated increases in both Greenland temperatures and precipitation over the anthropogenic period, Greenland temperature and accumulation reconstructions show no substantial increases during the anthropogenic period until the late twentieth century. These discrepancies suggest Greenland conditions during the twentieth century were driven either by natural variations of the North Atlantic climate (and the model's representation of the regional influences of greenhouse gases is inaccurate) or by greenhouse gas responses in conjunction with counteracting physical processes. These counteracting physical processes could include modes of natural variability, which in simulations do not follow historical trajectories, or physical processes not modelled in CCSM3. In Fig. 5, the warming of T42_all_Crowley temperatures over the nineteenth and twentieth centuries is interrupted by a few pauses, early in the twentieth century and most significantly from the 1950s to the 2000s. The first of these hiatuses is well-modelled by variations in the NAO–EA. The second appears to be due to other components of internal variability. Thus, internal variability is capable of obscuring the Greenland response to greenhouse gases over periods of a similar duration to those observed historically in these simulations. On the other hand, anthropogenic aerosols provide a plausible example of the latter processes, as they are not included in

the empirical model and only their direct effects are modelled in the simulations. In addition, simulated residuals exhibit some significant correlations with anthropogenic aerosols, but the sign and timing of these relationships depend on the variable being examined and the resolution. Furthermore, indirect effects of anthropogenic aerosols on clouds have been previously shown to generate significant multi-decadal variability in simulated North Atlantic SSTs (Booth et al. 2012). However, there is a degree of indeterminacy involved in trying to estimate the amplitude of an anthropogenic aerosol signal, since anthropogenic AODs and greenhouse gases are so well-correlated over the anthropogenic period. Thus, further analyses will need to be performed with models that include the indirect effects of anthropogenic aerosols to test whether these processes are indeed capable of providing counteracting influences to greenhouse gases over Greenland. Resolving the cause of the discrepancy between modelled and reconstructed Greenland conditions will be vital for correctly predicting future climate changes over Greenland and their effects on global sea levels.

Besides the lack of greenhouse gas signal in observational reconstructions, another major difference between the empirical estimates and the observational reconstructions is due to the NAO–EA exhibiting different correlation patterns for observed Greenland temperatures, accumulation, and the model. As a consequence, although this term reproduces much of the multi-decadal variability in the T42 simulations and to a lesser extent for the T85 simulations, it does not improve estimates of observed Greenland temperature and accumulation variability. Reversing the sign of the NAO–EA term improves the estimates for AND and BOX cases, to the degree that BOX accumulation estimates agree with observed reconstructions when the T42 parameters are employed. In this dataset, the NAO–EA is a better predictor of Greenland accumulation variability than the NAO alone.

Administraion Climate Program Office. (3) BOX: Obtained directly from Dr. J.E. Box.

References

Allan R, Ansell T (2006) A new globally complete monthly historical gridded mean sea level pressure dataset (HadSLP2): 1850–2004. J Clim 19:5816–5842

Andersen K, Ditlevson P, Rasmussen S, Clausen H, Vinther B, Johnsen S, Steffensen J (2006) Retrieving a common accumulation record from Greenland ice cores for the past 1800 years. J Geophys Res 111(D15):106

Andres HJ, Peltier WR (2013) Examining internal and external contributors to Greenland climate variability using CCSM3. J Clim 26:9745–9773

Booth BB, Dunstone NJ, Halloran PR, Andrews T, Bellouin N (2012) Aerosols implicated as a prime driver of twentieth-century North Atlantic climate variability. Nature 484:228–234

Box JE (2002) Survey of Greenland instrumental temperature records: 1873–2001. Int J Climatol 22:1829–1847

Box JE (2013) Greenland ice sheet mass balance reconstruction. Part II: Surface mass balance (1840–2010). J Clim 26:6974–6989

Box JE, Yang L, Bromwich DH, Bai LS (2009) Greenland ice sheet air temperature variability: 1840–2007. J Clim 22:4029–4049

Box JE, Cressie N, Bromwich DH, Jung JH, van den Broeke M, van Angelen J, Forster RR, Miege C, Mosley-Thompson E, Vinther B, McConnell JR (2013) Greenland ice sheet mass balance reconstruction. Part I: Net snow accumulation (1600–2009). J Clim 26:3919–3934

Chylek P, Folland C, Frankcombe L, Dijkstra H, Lesins G, Dubey M (2012) Greenland ice core evidence for spatial and temporal variability of the Atlantic Multidecadal Oscillation. Geophys Res Lett 39(L09):705

Clarke L, Edmonds HJ, Pitcher H, Reilly J, Richels R (2007) Scenarios of greenhouse gas emissions and atmospheric concentrations. Tech rep, Department of Energy, Office of Biological and Environmental Research, Washington, 7 DC, USA

Collins W, Bitz C, Blackmon M, Bonan G, Bretherton C, Carton J, Chang P, Doney S, Hack J, Henderson T, Kiehl J, Large W, McKenna D, Santer B, Smith R (2006) The community climate system model version 3 (CCSM3). J Clim 19:2122–2143

Compo G, Whitaker J, Sardeshmukh P, Matsui N, Allan R, Yin X, BE Gleason J, Vose R, Rutledge G, Bessemoulin P, Bronnimann S, Brunet M, Crouthamel R, Grant A, Groisman P, Jones P, Kruk M, Kruger A, Marshall G, Maugeri M, Mok H, Nordli O, Ross T, Trigo R, Wang X, Woodruff S, Worley S (2011) Review article the twentieth century reanalysis project. Q J R Meteorol Soc 137:1–28

Crowley T, Zielinski G, Vinther B, Udisti R, Kreutz K, Cole-Dai J, Castellano E (2008) Volcanism and the little ice age. PAGES Newsl 16:22–23

Fettweis X (2007) Reconstruction of the 1979–2006 Greenland ice sheet surface mass balance using the regional climate model MAR. Cryosphere 1:21–40

Fettweis X, Hanna E, Lang C, Belleflamme A, Erpicum M, Gallee H (2013) Important role of the mid-tropospheric atmospheric circulation in the recent surface melt increase over the Greenland ice sheet. Cryosphere 7:241–248

Flato G, Marotzke J, Abiodun B, Braconnot P, Chou S, Collins W, Cox P, Driouech F, Emori S, Eyring V, Forest C, Gleckler P, Guilyardi E, Jakob C, Kattsov V, Reason C, Rummukainen M (2013) Evaluation of climate models. In: Stocker T, Qin D, Plattner GK, Tignor M, Allen S, Boschung J, Nauels A, Xia Y, Midgely P (eds) Climate change 2013: the physical science basis. Contribution of working group I to the fifth assessment report of the intergovernmental panel on climate change. Cambridge University Press, Cambridge, pp 746–866

Frauenfeld OW, Knappenberger PC, Michaels PJ (2011) A reconstruction of annual Greenland ice melt extent, 1784–2009. J Geophys Res 116(D08):104

Gao C, Robock A, Ammann C (2008) Volcanic forcing of climate over the past 1500 years: an improved ice core-based index for climate models. J Geophys Res 113(D23):111

Hadley Centre for Climate Prediction and Research, Met Office, Ministry of Defence, United Kingdom (2000, updated monthly) Met Office Hadley Centre mean sea level pressure dataset. http://rda.ucar.edu/datasets/ds277.4/. Accessed 30 Jul 2013

Hanna E, Cappelen J (2003) Recent cooling in coastal southern Greenland and relation with the North Atlantic Oscillation. Geophys Res Lett 30:1132

Hanna E, Huybrechts P, Janssens I, Cappelen J, Steffen K, Stephens A (2005) Runoff and mass balance of the Greenland ice sheet: 1958–2003. J Geophys Res 110(D13):108

Hanna E, Huybrechts P, Steffen K, Cappelen J, Huff R, Shuman C, Irvine-Fynn T, Wise S, Griffiths M (2008) Increased runoff from melt from the Greenland ice sheet: a response to global warming. J Clim 21:331–341

Hanna E, Huybrechts P, Cappelen J, Steffen K, Bales RC, Burgess E, McConnell JR, Steffensen JP, van den Broeke M, Wake L, Bigg G, Griffiths M, Savas D (2011) Greenland ice sheet surface mass balance 1870 to 2010 based on twentieth century reanalysis, and links with global climate forcing. J Geophys Res 116(D24):121

Hanna E, Fettweis X, Mernild SH, Cappelen J, Ribergaard MH, Shuman CA, Steffen K, Wood L, Mote TL (2014) Atmospheric and oceanic climate forcing of the exceptional Greenland ice sheet surface melt in summer 2012. Int J Climatol 34:1022–1037

Johnsen S, Dansgaard W, White J (1989) The origin of Arctic precipitation under present and glacial conditions. Tellus 41B:452–468

Kobashi T, Goto-Azuma K, Box J, Gao CC, Nakaegawa T (2013a) Causes of Greenland temperature variability over the past 4000 year: implications for northern hemispheric temperature changes. Clim Past 9:2299–2317

Kobashi T, Shindell D, Kodera K, Box J, Nakaegawa T, Kawamura K (2013b) On the origin of multidecadal to centennial Greenland temperature anomalies over the past 800 year. Clim Past 9:583–596

Krueger O, Schenk F, Feser F, Weisse R (2013) Inconsistencies between long-term trends in storminess derived from the 20CR reanalysis and observations. J Clim 26:868–874

Luthcke SB, Sabaka T, Loomis B, Arendt A, McCarthy J, Camp J (2013) Antarctica, Greenland and Gulf of Alaska land-ice evolution from an iterated GRACE global mascon solution. J Glaciol 59:613–631

Meehl GA, Washington WM, Arblaster JM, Hu A, Teng H, Kay JE, Gettelman A, Lawrence DM, Sanderson BM, Strand WG (2013) Climate changes projections in CESM1(CAM5) compared to CCSM4. J Clim 26:6287–6308

NCDC/NESDIS/NOAA/US Dept of Commerce (2012, updated monthly) NCDC Global Historical Climatology Network Monthly Version 3 (GHCNMV3). http://rda.ucar.edu/datasets/ds564.1/. Accessed 30 Jul 2013

NCDC/NESDIS/NOAA/US Dept of Commerce, Carbon Dioxide Information Analysis Center/Environmental Sciences Division/ Oak Ridge National Laboratory/US Dept of Energy, and Office of Climatology/Arizona State University (1995, updated quarterly) Global Historical Climatology Network (GHCN) Version 2 Temperature, precipitation, pressure. http://rda.ucar.edu/datasets/ds564.0/. Accessed 30 Jul 2013

NOAA/NWS/CPC (2013a) East Atlantic Teleconnection Pattern. http://www.cpc.ncep.noaa.gov/data/teledoc/ea.shtml

NOAA/NWS/CPC (2013b) North Atlantic Oscillation. http://www.cpc.ncep.noaa.gov/data/teledoc/nao.shtml

NOAA/NWS/CPC (2013c) Teleconnection Index calculation procedures. http://www.cpc.ncep.noaa.gov/data/teledoc/teleindcalc.shtml

Peltier WR (2009) Closure of the budget of global sea level rise over the GRACE era: the importance and magnitudes of the required corrections for global glacial isostatic adjustment. Quat Sci Rev 28:1658–1674

Ramaswamy V, Boucher O, Haigh J, Hauglustaine D, Haywood J, Myhre G, Nakajima T, Shi G, Solomon S (2001) Radiative forcing of climate change. In: Houghton J, Ding Y, Griggs D, Noguer M, van der Linden P, Dai X, Maskell K, Johnson C (eds) Climate change 2001: the scientific basis. Contribution of working group 1 to the third assessment report of the intergovernmental panel on climate change. Cambridge University Press, Cambridge, pp 349–416

Riahi K, Gruebler A, Nakicenovic N (2007) Scenarios of long-term socio-economic and environmental development under climate stabilization. Technol Forecast Social Change 74:887–935

Roy K, Peltier WR (2011) GRACE era secular trends in Earth rotation parameters: A global scale impact of the global warming process? Geophys Res Lett 38(L10):306

Sen A, Srivastava M (1990) Regression analyses: theory, methods, and applications. Springer, New York

Smith S, Wigley T (2006) Multi-gas forcing stabilization with the MiniCAM. Energy J Spec Issue 3:373–391

Stroeve J, Holland MM, Meier W, Scambos T, Serreze M (2007) Arctic sea ice decline: Faster than forecast. Geophys Res Lett 34(L09):501

Swingedouw D, Terray L, Cassou C, Voldoire A, Salas-Melia D, Servonnat J (2011) Natural forcing of climate during the last millennium: fingerprint of solar variability. Clim Dyn 36:1349–1364

Taylor K, Stouffer R, Meehl G (2009) An overview of CMIP5 and the experiment design. Bull Am Meteorol Soc 93:485–498

Vavrus S, Holland M, Jahn A, Bailey D, Blazey B (2012) Twenty-first-century Arctic climate change in CCSM4. J Clim 25:2696–2710

Velicogna I, Wahr J (2013) Time-variable gravity observations of ice sheet mass balance: precision and limitations of the GRACE satellite data. Geophys Res Lett 40:3055–3066

Vettoretti G, Peltier WR (2013) Last Glacial Maximum ice sheet impacts on North Atlantic climate variability: the importance of the sea ice lid. Geophys Res Lett 40:6378–6383

Wake L, Huybrechts P, Box J, Hanna E, Janssens I, Milne G (2009) Surface mass-balance changes of the Greenland ice sheet since 1866. Ann Glaciol 50:178–184

Wise M, Calvin K, Thomson A, Clarke L, Bond-Lamberty B, Sands R, Smith S, Janetos A, Edmonds J (2009) Implications of limiting CO2 concentrations for land use and energy. Science 324:1183–1186

Woollings T, Hannachi A, Hoskins B (2010) Variability of the North Atlantic eddy-driven jet stream. Q J R Meteorol Soc 136:856–868